



HAL
open science

Growth mechanism and repassivation kinetic determinations on stainless steel under sliding: Role of the solution pH and dissolved oxygen concentration

Nicolas Mary, Benoit Ter-Ovanessian, Bernard Normand

► To cite this version:

Nicolas Mary, Benoit Ter-Ovanessian, Bernard Normand. Growth mechanism and repassivation kinetic determinations on stainless steel under sliding: Role of the solution pH and dissolved oxygen concentration. *Wear*, 2020, 460-461, pp.203478. 10.1016/j.wear.2020.203478 . hal-03345104

HAL Id: hal-03345104

<https://hal.science/hal-03345104>

Submitted on 26 Sep 2022

HAL is a multi-disciplinary open access archive for the deposit and dissemination of scientific research documents, whether they are published or not. The documents may come from teaching and research institutions in France or abroad, or from public or private research centers.

L'archive ouverte pluridisciplinaire **HAL**, est destinée au dépôt et à la diffusion de documents scientifiques de niveau recherche, publiés ou non, émanant des établissements d'enseignement et de recherche français ou étrangers, des laboratoires publics ou privés.



Distributed under a Creative Commons Attribution - NonCommercial 4.0 International License

1 **Growth mechanism and repassivation kinetic determinations on stainless**
2 **steel under sliding: role of the solution pH and dissolved oxygen**
3 **concentration.**

4

5 *Nicolas Mary¹, Benoit Ter-Ovanessian¹, Bernard Normand¹*

6 ¹ Université de Lyon, INSA Lyon, CNRS, MATEIS UMR 5510, F-69621 Villeurbanne Cedex France

7

8 **Abstract**

9 The tribo electrochemical behavior of 2205 duplex stainless steel had been studied under acidic and
10 neutral solutions with control of the dissolved dioxygen. The study focused on the oxide film
11 formation using a galvanic technique approach implemented in a tribometer. Higher wear rates were
12 measured in low pH and aerated solution. In low O₂ concentration, a wear reduction was observed
13 for each pH. Analysis of the passivation transients showed the pH influence on the oxide growth
14 mechanism, irrespective of the O₂ level. Temporal analysis of the transients confirmed the faster
15 passivation of the wear track in acidic solution. In a controlled O₂ environment, the nucleation and
16 the oxide growth were slow down, irrespective of pH. The degradation rate was then correlated to
17 the passivation kinetic and the aging of the passive film.

18

19

20

21

22 **Keywords:**

23 Tribocorrosion, repassivation kinetic, dissolved dioxygen and pH, repassivation modeling

24

25 1. Introduction

26 Passive materials as stainless steels are corrosion resistant as long as an oxide-hydroxide film covers
27 their surfaces [1,2]. In a corrosive solution, the dissolution kinetics of the surface mainly depends on
28 the material chemistry (chromium content) and the oxidizing power of the solution (pH, chloride
29 concentration, electrode potential) [3–5]. When the surface is scratched, the oxide layer is broken,
30 and the bulk material dissolves. In most cases, a new film grows shortly after and limits surface
31 oxidation [3]. An overall degradation is usually expected in tribocorrosion as mechanic and
32 environment act synergistically [6–8].

33 In previous work, the authors discussed the influence of the applied potential on the corrosion wear
34 resistance of **ferritic stainless steel** [5]. As the potential goes to the anodic domain, the oxide film
35 becomes **thicker**, and the wear increases. It originates from the higher dissolution rate of the oxide-
36 free surface and the role of oxide debris in the contact [6,9,10]. Other works pointed out the
37 mitigation of wear in basic solution due to a lower surface dissolution and higher deformability of the
38 oxide on the worn surface [11]. **For Ruiz-Andres et al. [12] and Garcia et al. [13], the contact**
39 **frequency (i.e., the inverse of the elapsed time between two contacts at a given point) is the main**
40 **mechanical parameter as it plays a role on the formation, the growth and the aging of the oxide [14].**

41 In tribocorrosion, the surface reactivity is described from the current variation along with the test,
42 and it corresponds to the dissolution and the oxide film reformation [15]. High contact frequencies
43 promote dissolution and hinder the oxide film growth, consequently. It leads to a quasi-constant
44 current since the wear track remains permanently active [16]. At the opposite, current transients are
45 recorded for low contact frequencies. Each transient is characterized **by a sharp** increase of the
46 current during sliding, **namely as depassivation current** and a decreasing step during the latency
47 period, referred to as repassivation current [5]. The depassivation current is mostly controlled by the
48 corrosion behavior of the free oxide surface and depends on the chemical composition of the
49 material, the solution, and the mechanical load [16,17]. The repassivation current characterizes the

50 ability of the oxide growth on a deformed surface. Earlier, Olsson et al. [18] and Jemmely et al. [8]
 51 analyzed such transients based on the Interface Field Model and High Field Model, respectively. They
 52 show a time dependence with the mechanical parameters, such as the speed motion of pin, the pin
 53 load, the lubricant, and solution chemistry and also with the applied potential. Their investigations
 54 also indicated that the grow mechanism is affected by the charge transfer coefficient of oxidation
 55 reactions, which might be related to the oxide grow mechanism. However, Goldberg et Gilbert [19]
 56 suggested that the dissolved oxygen might not have a direct effect on the oxide film rebuilt in
 57 tribocorrosion.

58 By the past, Okorie et al. [20] have demonstrated that the kinetics of the oxide film formation can be
 59 defined from a two exponentials law (equation 1) where the first term characterizes the oxide film
 60 nucleation kinetic (time constant τ_{2D}) and the second term quantifies the oxide thickening rate (time
 61 constant τ_{3D}) [15,20]:

$$62 \quad i_t = i_{2D} \cdot \exp(-\pi\lambda^2 Nt) + i_{3D} \cdot \exp\left(-\frac{SD}{\delta \cdot \theta} \cdot t\right) + i_0 = i_{2D} \cdot \exp\left(-\frac{t}{\tau_{2D}}\right) + i_{3D} \cdot \exp\left(-\frac{t}{\tau_{3D}}\right) + i_0$$

63 Equation 1

64 In equation 1, λ is a constant dependent on the potential step, N is the number of nuclei initially
 65 formed, S is the surface area, δ is the boundary diffusion layer thickness, θ is the solution volume. i_{2D}
 66 and i_{3D} are functions of the potential in the film and the film resistance properties. i_0 was introduced
 67 to take into account the steady-state current of the passive film.

68 This approach was applied previously to characterize the oxide film kinetic during tribocorrosion at
 69 several applied potentials [5]. A faster repassivation kinetic was determined at higher anodic
 70 potentials. The role the microstructure was also highlighted: the oxide film rebuilt reduces for dual-
 71 phase steel because of the establishment of galvanic coupling between the two phases.

72 The present work aims to emphasize the role of the oxidizing power of a solution on the
 73 repassivation kinetics of a worn surface. For that purpose, a 2205 duplex stainless steel was selected

74 since this has several tribological and corrosion wear issues [21]. The mechanical configuration (for
75 example, nominal charge and contact properties) was kept constant between all experiments in
76 order to focus on the role of the environment. pH and dissolved oxygen are considered as the two
77 main parameters playing on the potential of the solution. On the one hand, tuning the pH is a way to
78 control the oxide film composition with an enrichment of the layer into iron in basic solution and to
79 mitigate the wear [7]. On the other hand, the dissolved dioxygen concentration changes the solution
80 potential and the cathodic reaction as the reduction of O₂ in a neutral solution. The present
81 tribocorrosion tests are performed in a galvanic coupling condition where the DSS2205 is connected
82 to a graphite counter electrode to enhance the effect of the oxidizing power of the solution. With
83 this setup, no absolute values can be extracted since it is not representative of a real case, but
84 comparisons between several conditions can be made, and the results can be discussed in terms of
85 factors of influence. A second advantage is to record the potential and the current fluctuation
86 simultaneously during sliding that express the electrochemical reactivity of the worn surface as a
87 function of the environment.

88

89 2. Experimental procedures

90 Working electrodes were made from a commercial duplex stainless steel (DSS2205) with a classical
91 austenite-ferrite lamellar microstructure obtained from the rolling process. Note that no additional
92 treatment was performed on stainless steel. Chemical composition of significant elements which are
93 usually involved in the passivation behavior of stainless steel was determined by EDX measurements
94 (average values from 4 surfaces of 200 x 200 μm²) : 0.02 wt.% C, 5.45 wt.% Ni, 22.62 wt.% Cr, 1.65
95 wt.% Mn, 2.88 wt.% Mo, 0.47 wt.% Si, 0.17 wt.% N, 0.025 wt.% P, 0.21 wt.% Cu, 0.004 wt.% S and bal-
96 Fe. The surface of DSS2205 has been grinding with SiC papers until grit 4000 (SiC) in order to reduce
97 the initial roughness and get reproducible surface morphologies. The final grinding step was done
98 parallel to the sliding direction of the tribocorrosion experiments.

99 Tribocorrosion tests were performed with a reciprocating motion tribometer (Falex company),
100 already presented elsewhere [22]. Corundum alumina pin was selected in order to limit severe
101 adhesive wear usually observed in metal-metal contact [23]. This counter body also presents high
102 mechanical characteristics (Young's modulus 380 GPa, Poisson's ratio 0.25), and excellent chemical
103 resistance [24]. A tip curvature radius of 28 mm was obtained by polishing until SiC emery paper (Grit
104 4000) with a homemade pin holder. A normal force of 5N was applied for 3000 motions. This latter
105 had a stroke length of 2 mm (trapezoidal motion with a sliding speed of 50 mm/s) and a latency
106 period of 10 seconds. This duration was established from preliminary experiments to take into
107 account the time of double-layer charging and the repassivation [25]. According to the Hertz's elastic
108 theory, calculations give a maximum contact pressure of 280 MPa and a mean contract pressure of
109 190 MPa with a young's modulus of 190 GPa and Poisson's ratio of 0.3 for DSS2205. After sliding,
110 wear profiles were acquired from ex-situ contact profilometry measurements (Surfascan 2D,
111 Somicronic, Belgium). From the wear track width and depth measurements, the wear volume was
112 quantified by Equation 2 where the wear track is modeled by two semi-spherical tips and a half-
113 cylinder body [26,27]

$$114 \quad V_{tot} = \pi \cdot h^2 \cdot (R_c - h/3) + \frac{h}{6 \cdot l} \cdot (3 \cdot h^2 + 4 \cdot l^2) \cdot L \quad \text{Equation 2.}$$

115 Where h is the pin penetration depth (cm), R_c is the pin curvature radius (cm), L is the stroke length
116 (cm), and l is the track width (cm).

117 A specific tribocorrosion cell has been designed to ensure dissolved dioxygen control during
118 experiments (Figure 1a). Determination of O_2 concentration was done by a needle-type housing
119 fiber-optic oxygen connected to an OXY-MICRO-AOT provided by WPI-Europe with a detection limit
120 of 10 ppb. The oxygen sensor was located in the cell at 5 mm up to the working electrode and 1 cm
121 far from the wear track for tribocorrosion. In this cell, a Viton seal with an aperture allowing the pin
122 motion is fixed to the cell wall and mounted 2 mm above the solution level. The O_2 sensor is placed
123 at 1 cm to the pin and 1 mm to the sample surface to measure the level of dissolved dioxygen

124 accurately. For reducing the gas exchange between the cell and the lab, the seal aperture is adjusted
125 to the pin size, which introduces some friction points along with the pin motion. Therefore, the
126 determination of the tangential load is affected by the air barrier system, and the coefficient of
127 friction (COF) cannot be considered as relevant data even if some correction procedures were tested.
128 Additional developments are then required to record the COF.

129 Electrochemical and triboelectrochemical experiments were performed with the specific three
130 electrodes cell connected to GAMRY Ref600 potentiostat (volume of electrolyte = 15 cm³). The
131 working electrode was composed of the DSS2205 with an active surface of 3.7 cm². The counter
132 electrode was a graphite disc with a specific surface of 22 cm². Finally, a mercury sulfate electrode
133 (E=+0.65 V/SHE) was used as a reference electrode. In order to avoid localized corrosion, a solution
134 of 0.02M Na₂SO₄ with a natural pH of 6.5 was selected. From it, a second electrolyte was prepared by
135 H₂SO₄ addition to reach a pH of 1.5. Two oxygen concentrations were tested. A concentration of
136 6700 ppb was obtained by an air lab injection in the tribocorrosion cell, whereas a concentration of
137 lower than 50 ppb of O₂ was reached with argon injection. For both aerated and deaerated solutions,
138 gas sparking was kept active over the experiments. It reduces the mass transport effect on the redox
139 processes in addition to the pin motion effect. Moreover, it avoids cell re-oxygenation in deaerated
140 conditions.

141 For tribocorrosion experiments, working electrodes (DSS2205) and secondary electrodes were
142 connected through a zero-resistance ammeter (ZRA) to monitor simultaneously potential and current
143 variations during sliding [28]. This cell is a modified set-up proposed by Wu et al. [28], where the
144 surface ratio between the second electrode and the working electrode is fixed at 7 [29]. One of the
145 most critical parameters in galvanic corrosion is the electrode area ratio. Usually, rapid corrosion is
146 favored by a high cathode to anode ratio, whereas a high anode to cathode ratio leads to slow
147 corrosion. Consequently, the surface ratio has to be constant between all tests for comparative
148 studies. With our design, the worn surface always remains smaller than the overall cathodic surface
149 (graphite electrode and wear track surrounding). Since the DDS2205 is connected to the graphite

150 electrode, the reduction mainly takes place on the graphite surface since its potential is higher than
151 the DSS2205. Also, the overall cathodic surface remains larger than the anodic; therefore, the anodic
152 reaction may be supposed to be the limiting step in neutral and aerated solution [30,31]. Note that
153 the ohmic drop was quantified, and the potential drift was evaluated at $2 \times 10^{-6} V_{MSE}$, which can be
154 considered as negligible [8,18,31,32].

155 Before each experiment, an electrochemical pre-treatment was applied in order to increase the
156 reproducibility of experiments by controlling the initial surface reactivity [33]. It was carried out as
157 follows: (i) a potentiostatic step at +0.2 V for 300s, (ii) a cathodic polarization curve from +0.2 V to -
158 1.2 V at a scan rate of 0.15 mV/s. After, either polarization or tribocorrosion experiments were
159 performed. Potentiodynamic curves were plotted from -1.2 V until +0.6 V with a scan rate of 0.15
160 mV/s. They were used to describe the initial passivation ability of DSSS2005 as a function of the
161 oxygen concentration and the pH. Because both DSS2205 and the graphite counter electrode are in
162 the galvanic coupling, an initial delay is required to ensure the potential and current steady states
163 before the sliding begins. This latter was fixed at 70 000 seconds. Both potential and current were
164 recorded at a sample rate of 33 mHz to monitor the general evolution of galvanic coupling between
165 the two materials. Potential and current acquisition frequencies are increased until 100 Hz when the
166 sliding starts. This rate allows a good definition of the potential and current fluctuations for the fit
167 with equation 1 and the power law for the mechanism determination (as discussed in Part 3).

168

169 **3. Results and discussion**

170 **3.1. Passivation behavior of duplex stainless steel**

171 Figure 1b shows classical current evolution as a function of potential used to describe the passivation
172 ability of stainless steel. In the cathodic domain, the electrochemical behavior is dominated by the
173 solution pH rather than the dissolved oxygen, which leads to more cathodic corrosion potentials in

174 neutral than in acidic solution. The elimination of O₂ is found to influence the cathodic process [34].

175 The cathodic reaction in acidic and neutral solution is:

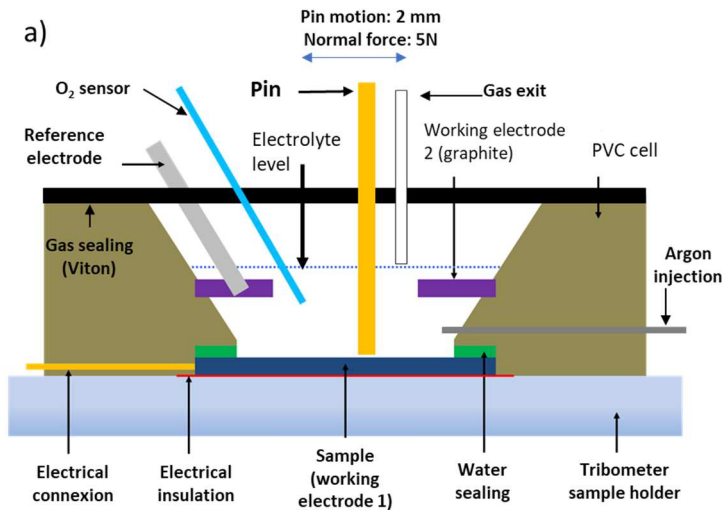


177 $E_{H_2O/O_2} = E_{H_2O/O_2}^\circ + \frac{RT}{4F} \ln \frac{p_{O_2}}{a_{H^+}^4}$ Eq. 4

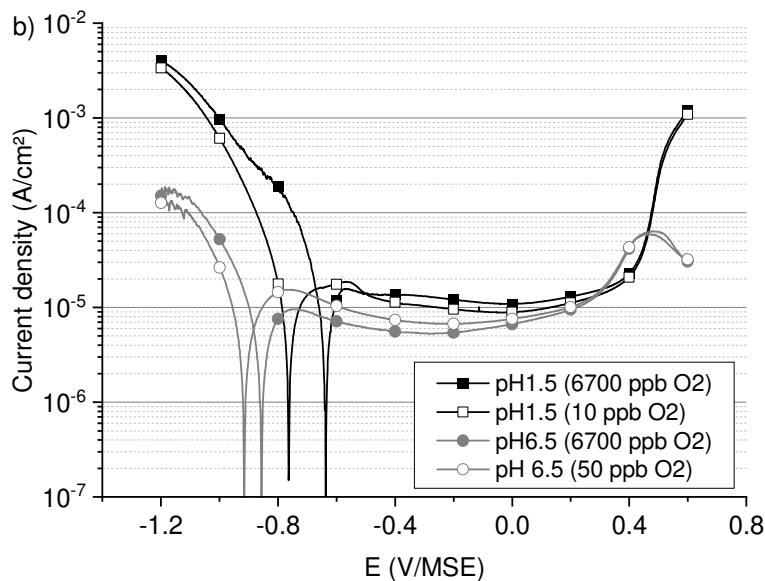
178 Where E_{H_2O/O_2} is the equilibrium potential, E_{H_2O/O_2}° is the standard equilibrium potential, T is the
179 temperature, R is gas constant, p_{O_2} is the oxygen partial pressure and a_{H^+} is the activity coefficient of
180 H⁺.

181 Thus, oxygen elimination decreases E_{H_2O/O_2} and move slightly the ideal polarization curve in the
182 negative direction and the corrosion potential to the cathodic domain. As already shown by Feng et
183 al. [34], dissolved oxygen has less influence on the anodic process since curves almost superpose.

184 For potentials higher than 0.4 V/MSE, the transpassive region is reached. It is characterized by an
185 active dissolution in low pH solution and an active-passive transition in neutral electrolyte. In the
186 passive region, all curves present a plateau in the range of -0.6 V/MSE to 0.4 V/MSE. Whatever the
187 level of dissolved oxygen, the current remains slightly lower in neutral solution ($\sim 5 \times 10^{-6}$ A/cm²) than
188 in acid solution (at approximately 10×10^{-6} A/cm²). It comes from the decrease of the dissolution rate
189 of the oxide layer by the stabilization of the iron species in a thicker film [35,36].



190



191

192 **Figure 1. a) Schematic representation of the tribo-electrochemical cell.** b) Polarization curves on
193 DSS2205 in acidic and neutral solutions in aerated and deaerated conditions.

194

195 3.2. Galvanic coupling between DSS2205 and graphite counter electrode

196 When DSS2205 is paired with the graphite disc, a galvanic coupling establishes between these two
197 electrodes. Figure 2 shows the galvanic potential and current stabilizations during the
198 electrochemical and chemical equilibriums setting up. From them, it can be assumed that the
199 galvanic coupling reaches a quasi-steady state after 7×10^4 seconds suggesting that surface reactivity

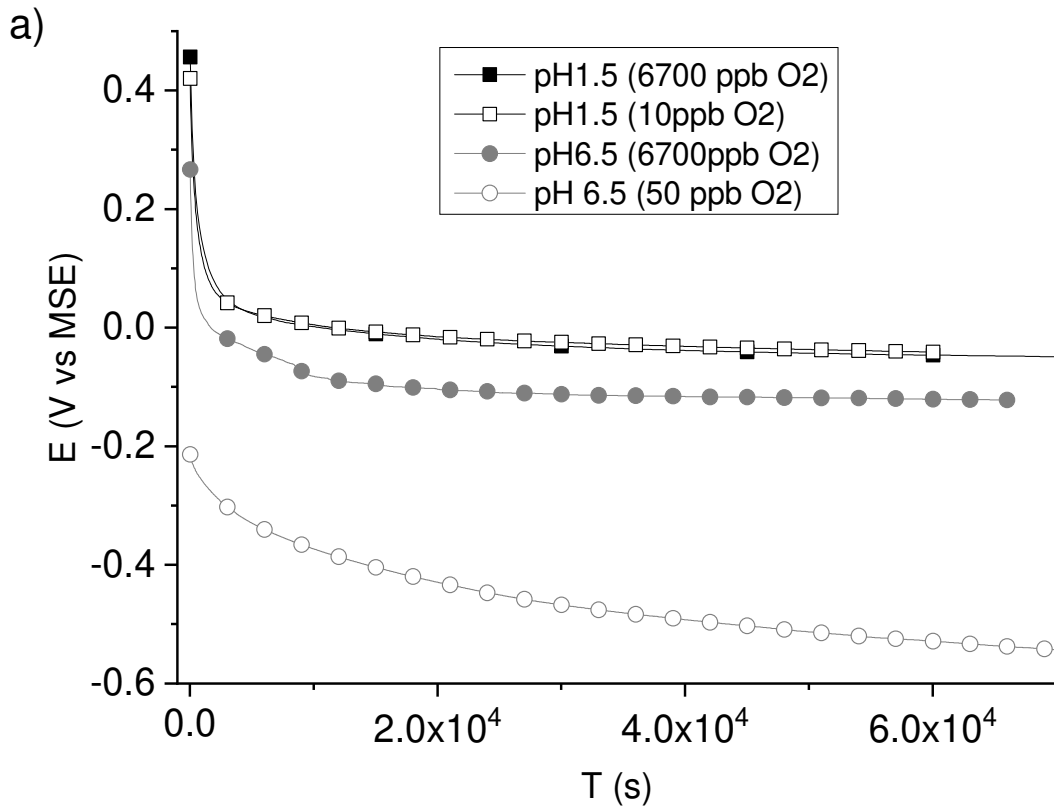
200 becomes constant over time. For all experiments, the potentials are located in the passive domain
201 (Figure 1b).

202 For galvanic coupling at pH 1.5, no apparent differences are observed on the potential and current
203 variations as a function of the oxygen level in the tribocorrosion cell (Figures 2a and 2b, respectively).
204 Potential stabilizes at approximately 0.0V/MSE, which corresponds to the minimum value of the
205 current density in the anodic domain of the polarization curves (Figure 1b). On the one hand, this
206 suggests that a dense oxide film could be formed on DSS2205 [36–38]. On the other hand, it suggests
207 that dissolved oxygen concentration should not play a direct role in the passivation mechanism. In
208 aerated solution at pH 6.5, the potential stabilizes at -0.1 V/MSE after 2×10^4 seconds (Figure 2a). This
209 value corresponds to that one at the minimum of the current density on the polarization curve
210 (Figure 1b). Then, a similar remark than in acidic solution can be made on the passive film properties:
211 when the O_2 level decrease in the cell, a shift of the corrosion potential is detected toward the
212 cathodic values (Figure 2a).

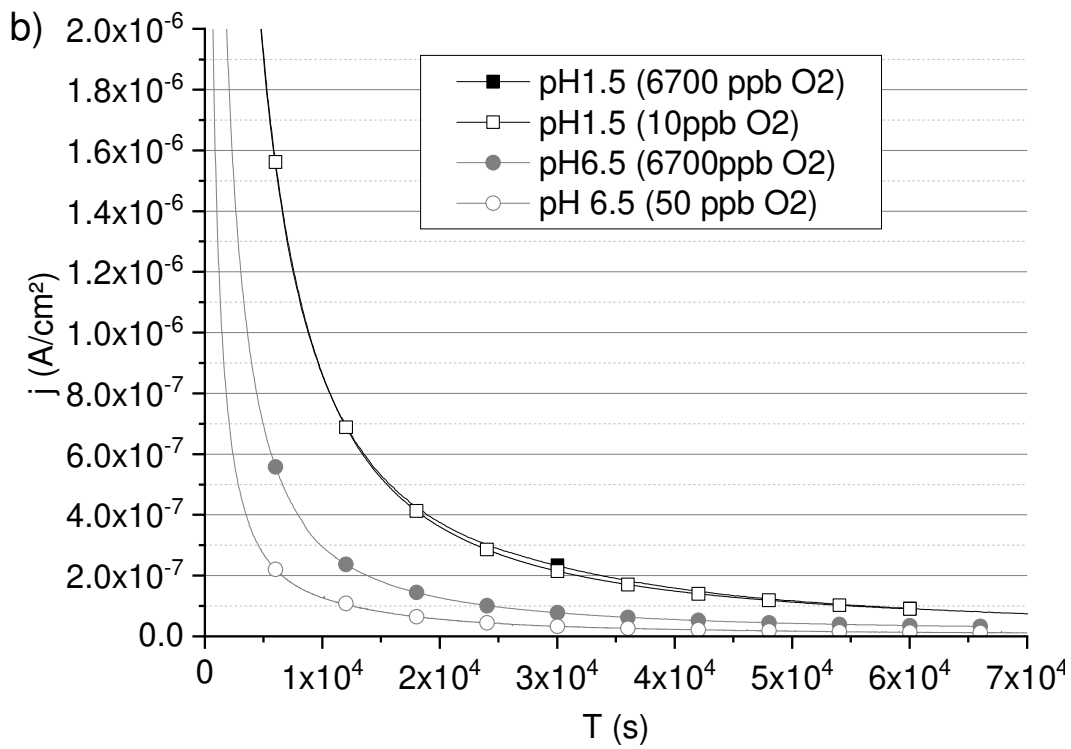
213 Figure 2b shows the current evolutions when the DSS2205 is immersed in solutions. High currents
214 are recorded at the earliest moment and then decrease rapidly. This trend corresponds to the
215 surface activation in solution followed by the formation and the stabilization of the oxide film. In
216 acidic solution, the surface passivation is slower because of the competition between the surface
217 dissolution and the oxide film nucleation and growth. In the neutral solution, the current plateau is
218 reached more rapidly since the material is less sensitive to dissolution. It is worth noticing that the O_2
219 level does not affect the current decreases in the acidic environment while it shortens the current fall
220 in the neutral solution. Current densities reach about 1×10^{-7} A/cm² after 4×10^4 seconds, and the
221 effects of the pH or O_2 level are not anymore visible. Both potential and current evolutions confirm a
222 modification of kinetic reactions linked to the contribution of either anodic reactions (metal
223 dissolution) or cathodic reactions (such as oxygen mass transport under 6700 ppb O_2 or the charge
224 transfer of hydrogen or O_2 with few tens ppb O_2) [39].

225 Thus, the passivation ability of DSS2205 is not lost either by the stainless-steel coupling with the
226 graphite counter electrode or the solution conditions (pH or O₂ concentration). Moreover, the
227 continuous evolutions of both potential and current confirm the absence of crevice corrosion or
228 corrosion mechanism by differential aeration. These two corrosion processes have to be avoided
229 because they could induce strong current and potential fluctuations during the repassivation process
230 and generate significant errors on the times constant and growth mechanism determinations.

231



232



233

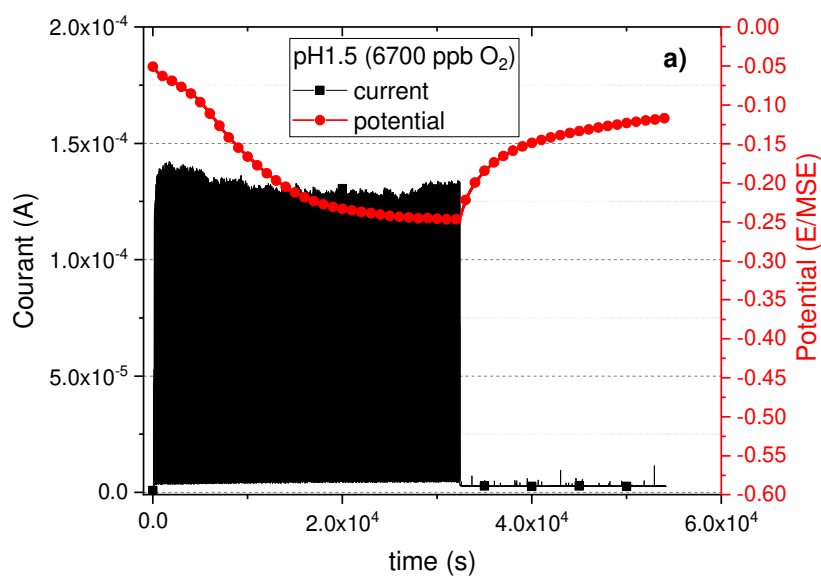
234 Figure 2. a) Potential and b) current density variations during galvanic coupling between DSS2005
 235 and graphite electrode in acid, neutral solutions in presence or not of dissolved oxygen.

236

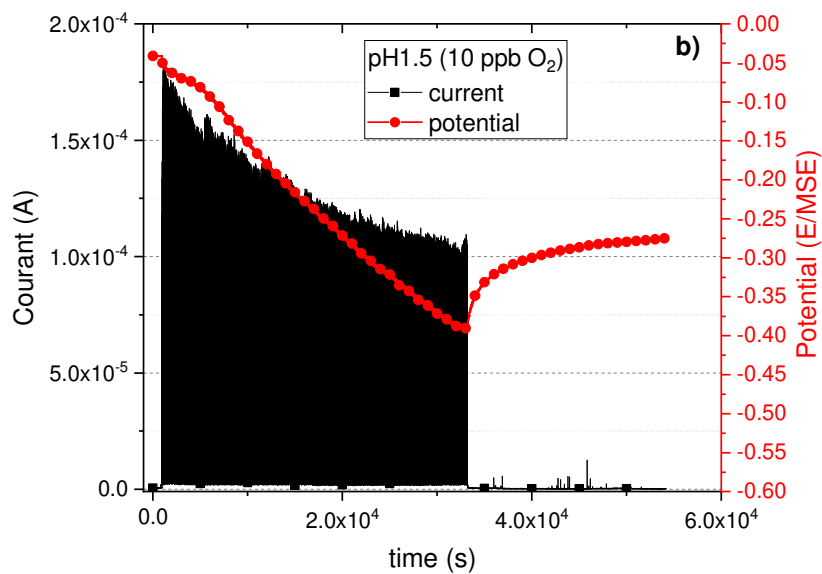
237 **3.2. Electrochemical behavior during sliding.**

238 In tribocorrosion, the potential variation reflects the surface reactivity. According to the mechanical
239 properties of the contact, the passive film is completely removed during sliding [31,40]. The surface
240 activation is confirmed by the potential drop toward cathodic values (Figure 3). However, this
241 evolution is not endless, and an equilibrium state under sliding can be reached.

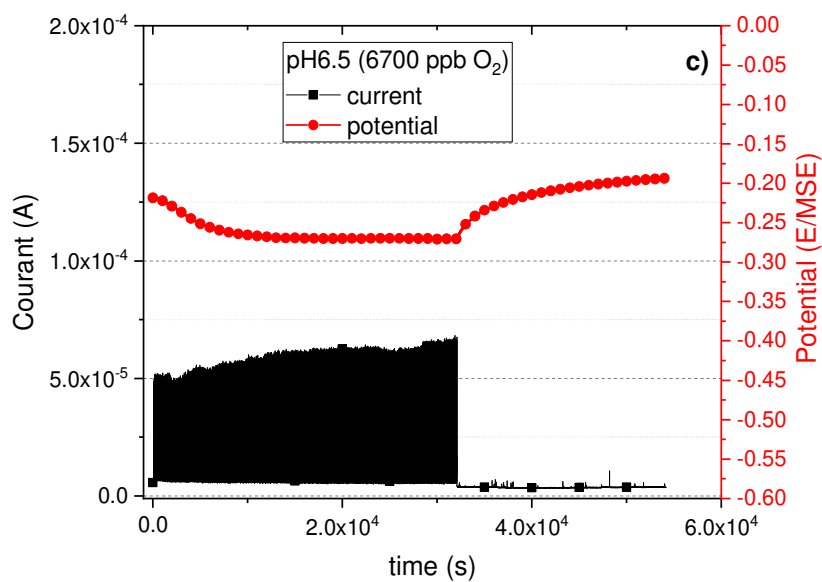
242 If the potential before sliding is independent of the O₂ concentration in acid, the surface activation by
243 sliding leads to a more substantial decrease of the potential in a low dissolved O₂ environment. The
244 potential stabilizes at -0.25V/MSE under 6700 ppb of O₂, whereas it decreases gradually with 10 ppb
245 of O₂ in the solution. Note that 3000 pin motions were not enough to get the equilibrium state under
246 sliding. A potential estimation was then done by adjusting the experimental curve by a logarithmic
247 law similar to that one proposed in [30]. In the end, the calculation gives an expected potential at
248 approximately -1.1 V/MSE. According to the thermodynamic tables, this latter is close to the Fe/Fe(II)
249 standard potential. To the opposite, the potential drop is less marked in neutral solution (in the
250 range of 0.05 V) than in acid and whatever the O₂ level. Therefore, the dissolved dioxygen in neutral
251 solution mostly affects the initial potential.



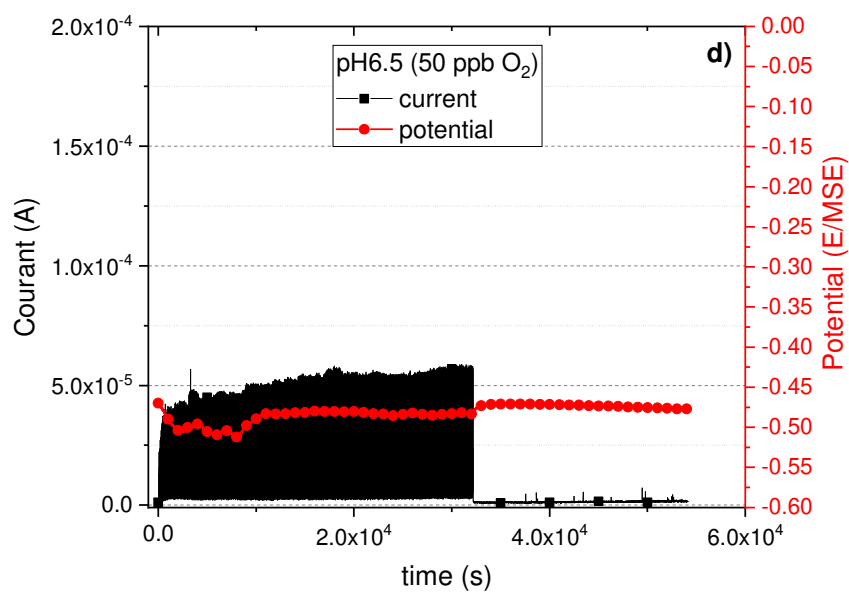
252



253



254



255

256 Figure 3. Potentials and current evolution during tribocorrosion experiments performed in pH 1.5 a)
257 6700 ppb O₂, b) 10 ppb O₂, and in pH 6.5 c) 6700 ppb O₂ and d) 50 ppb O₂.

258

259 Figure 3 also reports the general current variations as a function of the solution. Each curve
260 represents the sum of the depassivation (current increase) and the repassivation period (current
261 decrease) for 3000 slidings. For each experiment, the maximum current depends on the solution
262 properties (pH, O₂), which affect the electrochemical reactivity of the surface. Figure 3 shows a
263 stronger dissolution in acidic than in neutral solution (current intensity at approximately 7×10^{-5} A and
264 5×10^{-5} A, respectively). This difference is consistent with the lower passivation ability of the DSS2205
265 in pH 1.5, as already observed on polarization curves (Figure 1b). In the neutral solution, the current
266 is not changed by the level of dissolved, which is coherent with the direct stabilization of the
267 potential, even if the values of the potentials are not similar (Figure 3c and Figure 3d). At the end of
268 experiments, all currents drop to stable values at approximately 10×10^{-6} A, indicating that the wear
269 tracks recover a passive state.

270 The overall analysis of the current vs. time curves is then not selective enough to fully understand
271 the role of the pH and the O₂ level. Therefore, mechanistic and kinetic analyses are performed after
272 that on each repassivation transient [25]. On the one hand, the growth mechanism should be
273 sensitive to the solution pH (diffusion/migration of chromium and iron through the oxide layer). On
274 the other hand, the dissolved oxygen should play either a direct role in the mechanism of passivation
275 and the kinetic of the passivation or only have an indirect role in the repassivation kinetic due to a
276 modification of the oxidant property of the solution (Eq. 4) [19].

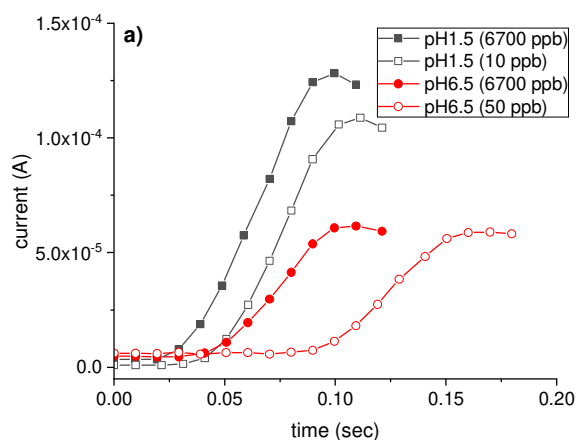
277

278 **3.3. Dissolution rate and corrosion wear.**

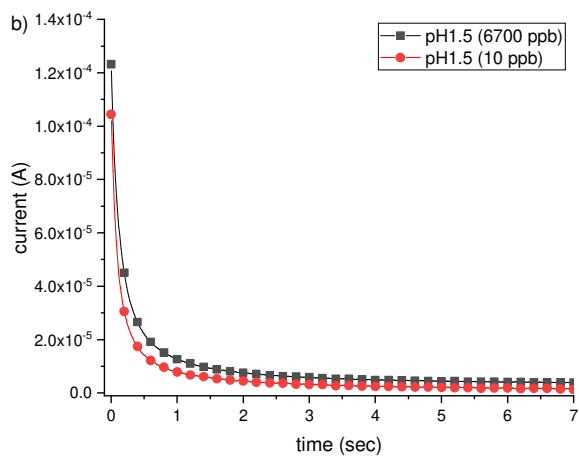
279 At the steady-state, the metal dissolution is limited by the presence of the oxide film in which
280 diffusion/migration of defects occurs. In tribocorrosion, the solution agitation and the generation of

281 a fresh surface modify the previous kinetic and thermodynamic equilibrium. The agitation directly
282 acts on the mass transport limitation (usually the dissolved dioxygen) at the cathodic region, and the
283 electrochemical behavior of the surface is driven by the dissolution of the oxide-free surface during
284 sliding. During sliding, the bare metal oxides, and the current increases (Figure 4a). In this study, the
285 mechanical contact properties are fixed, which means the interaction between the metal and the
286 solution controls the dissolution. Whatever the dissolved dioxygen, the depassivation rate ($\Delta i/\Delta t$) is
287 equal to $2.0 \pm 0.2 \times 10^{-3}$ A/s in acidic solution and it reduces to $0.9 \pm 0.2 \times 10^{-3}$ A/s in neutral solution
288 (Figure 4a). Note that these values are an average of the last 500 transients. The free-oxide surface
289 dissolution is then lower in neutral solution, as suggested in Figure 1b. Moreover, the non-
290 contribution of the dissolved dioxygen is confirmed during the dissolution. Consequently, the
291 modification of the oxidizing power of the solution by pH variation has a greater effect on the worn
292 surface reactivity than if the O_2 concentration varies. Repassivation current transients are reported in
293 Figures 4b and 4c for experiments performed in acidic and neutral solutions, respectively. Whatever
294 the condition, a current fall is recorded, indicating the passive behavior of the worn surface. An oxide
295 film nucleates and grows to limit the surface dissolution leading to a current fall. A more detailed
296 analysis of the current fall is provided in Part 3.4.

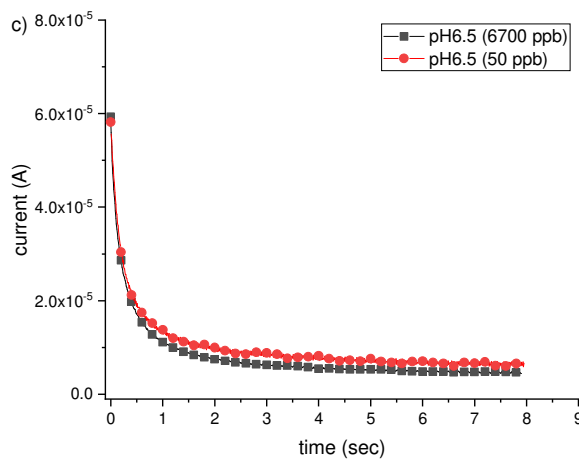
297



298



299



300

301 Figure 4. Current versus time curves during a) the depassivation (i.e., pin sliding) and the latency
 302 period in b) pH1.5 and c) pH 6.5 solutions. Example of transient number 2226 (i.e., after 2.2×10^4
 303 seconds of sliding).

304

305 Assuming the metal dissolution is equal to the electrical charge during only the depassivation (Q_{diss}),
 306 the chemical wear (V_{chem}) can be estimated by the Faraday law for a stainless steel with an equivalent
 307 molar weight of 55.07 g/mol and an equivalent electron number of 2.19 [25,41]. In aerated solution
 308 (Table 1), the chemical wear and the total wear decrease with pH as already reported by [11,42].
 309 Since the contribution of the chemical wear in the total wear is lower than 8.4% (Table 1), the total

310 wear is controlled by the mechanical properties of the contact. The wear reduction with the increase
311 of pH is then attributed to the oxide layer in the contact. A chromium oxide film is expected at pH
312 1.5, whereas a mixed iron-chromium oxide-hydroxide film grows in a neutral solution. The
313 breakdown of the oxide layer generates hard debris that enhances the wear in pH 1.5, whereas the
314 wear volume remains lower because of the highest deformability of the oxide-hydroxide layer at pH
315 6.5. The decrease of the dissolved dioxygen does not significantly affect the chemical wear, as
316 reported in Table 1. However, the wear (V_{tot}) mitigates with the reduction of O_2 . If a direct effect is
317 not seen, a modification of the oxide composition is expected. Kuang et al. [43] shown a chromium
318 enrichment in the oxide with the dissolved oxygen decrease. Huang et al. [44] observed a
319 modification of the iron oxide composition from lepidocrocite to magnetite with the diminution of
320 O_2 . In deaerated solution, the total wear decreases of $11.3 \times 10^{-5} \text{ cm}^3$ and $3.4 \times 10^{-5} \text{ cm}^3$ in acidic and
321 neutral solutions, respectively. The chemical wear contribution in the total wear increases in low
322 concentration of dissolved dioxygen since the chemical wear remains at about $6.0 \times 10^{-7} \text{ cm}^3$ in pH 1.5
323 and $\sim 3.0 \times 10^{-7} \text{ cm}^3$ in pH 6.5. Table 1 shows a significant increase in the chemical wear in acidic
324 deaerated solution, which can be related to the more significant potential drop in pH 1.5 10 ppb O_2
325 leading to a more active surface. It is worth noting that the material deterioration is still dominated
326 by the contact properties where the oxide layer plays a limited role. Such behavior frequently
327 happens for high mechanical loads. Therefore, a decrease in the contact load may balance the
328 chemical contribution to the overall degradation.

329

330 Table 1. Quantification of the dissolution charge (Q_{diss}), chemical volume (V_{chem}), and the total wear
331 (V_{tot}) for experiments in aerated and deaerated solutions at pH1.5 and pH6.5. The contribution of the
332 chemical wear ($\% V_{chem}$) in the total wear is also reported.

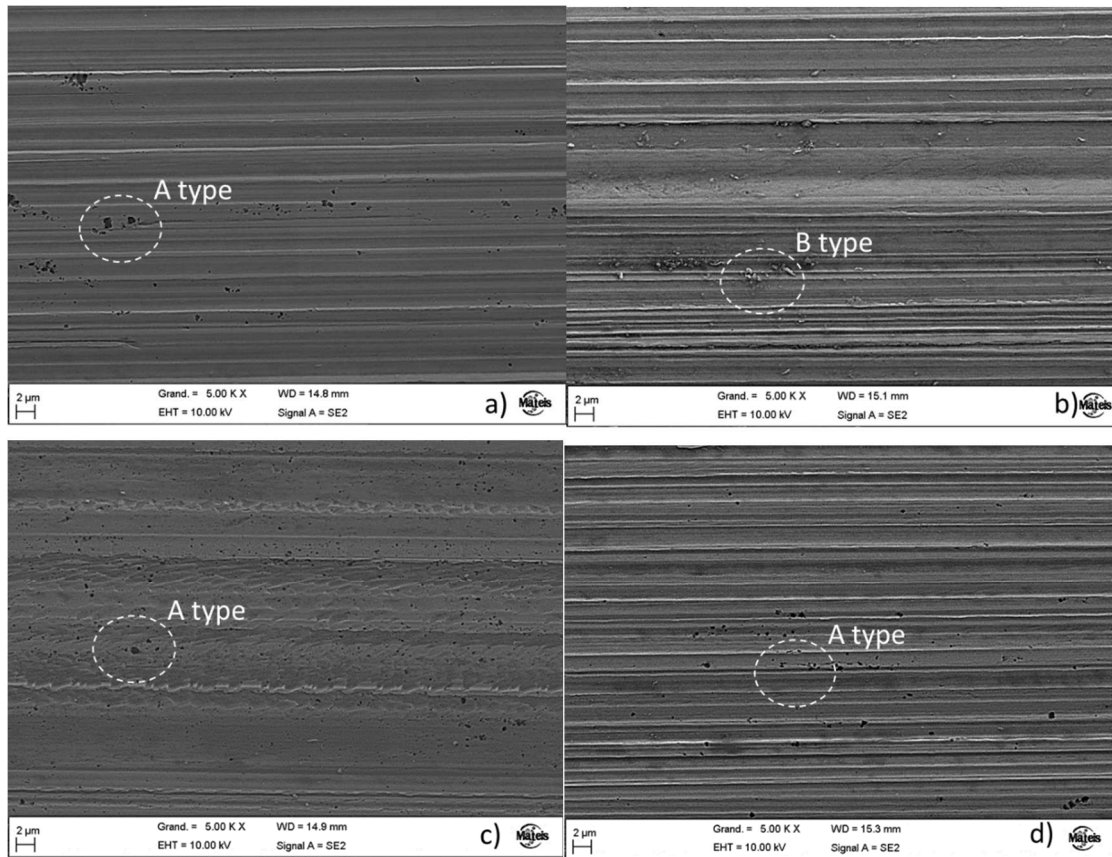
pH	O_2 (ppb)	Q_{diss} (C)	V_{chem} (cm^3)	V_{tot} (cm^3)	$\% V_{chem}$ in total wear
----	----------------	-------------------	---------------------------------	--------------------------------	--------------------------------

1.5	6700	0.017	5.7×10^{-7}	12.1×10^{-5}	0.5
	10	0.019	6.6×10^{-7}	0.8×10^{-5}	8.4
6.5	6700	0.009	3.3×10^{-7}	4.9×10^{-5}	0.7
	50	0.008	2.8×10^{-7}	1.5×10^{-5}	1.9

333

334 The worn surfaces then change with the oxide film composition (Figure 5). Parallel scratches to the
335 sliding direction indicate a scoring by abrasive wear whatever the test. Note that black debris (label
336 A-type) are detected except in aerated pH 6.5 (label B type). Chemical analysis by EDX gives a signal
337 of Al that comes from the pin. Indeed, mechanical degradation of the corundum pin occurs even if a
338 material transfer is observed (images not shown here). In aerated pH 6.5, the B-type debris is
339 identified as oxide particles detached from the wear track. These debris are evidence for a
340 modification of the oxide layer composition and mechanical properties with pH. In low dissolved
341 dioxygen, plastic flow is observed at pH 1.5, which contrasts with the abrasive wear in aerated
342 solution. Even if the potential drop to cathodic values, the current remains lower than under 6700
343 ppb O₂. These two observations lead to consider a modification of the passive film composition with
344 the environment. A similar conclusion is done in pH 6.5 with the absence of oxide debris, the
345 incorporation of Al in the wear track, and a lower potential in aerated solution. Further investigations
346 on oxide film are required to better understand the role of dissolved dioxygen on it and the wear
347 resistance. Assuming that the oxide film could change with the environment, the analysis of the
348 repassivation current has to be performed to detect any changes in the growth mechanism and the
349 growth kinetic.

350



351

352

353 Figure 5. SEM images of DSS2205 worn surface in a) pH 1.5 and b) pH 6.5 aerated solutions and c) pH
 354 1.5 and d) pH 6.5 deaerated solutions.

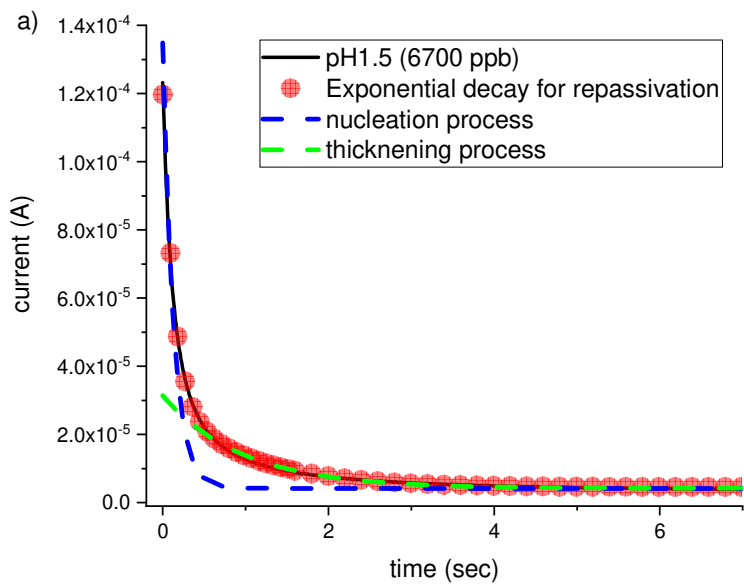
355

356 3.4. Quantification of the oxide nucleation and thickening kinetics

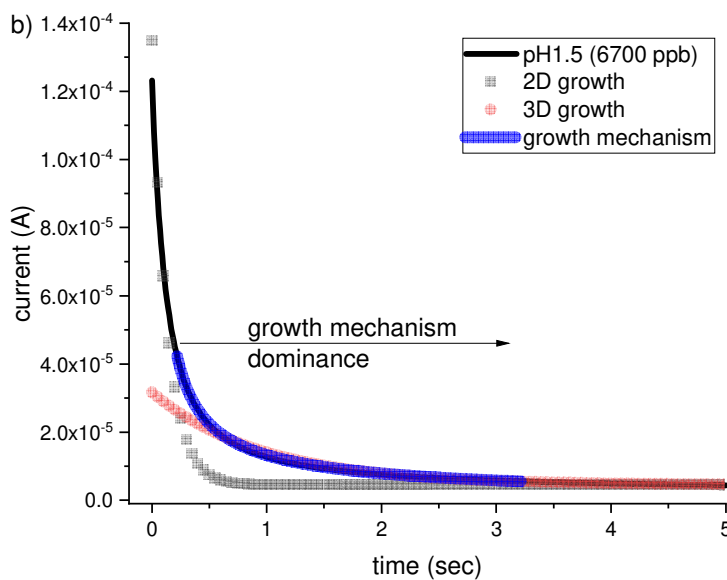
357 For stainless steel, the determination of the chemical composition of the oxide layer is usually
 358 performed by surface analysis, and it shows the promotion of a Cr_2O_3 layer in acidic solution. In
 359 contrast, a mix of chromium and iron structure develops for higher pH [1,45]. Because the chromium
 360 and iron affinities with oxygen are not equivalent (i.e., $\Delta H_f^\theta (\text{Cr}_2\text{O}_3) = 1139.7 \text{ kJ/mol}$ and ΔH_f^θ
 361 $(\text{Fe}_2\text{O}_3) = 824.2 \text{ kJ/mol}$ [46]), an effect on the repassivation kinetic is expected. Repassivation
 362 transients were then fitted with Equation 1 to extract the time constants for the 2D nucleation (τ_1)
 363 and the 3D thickening (τ_2) rates of the oxide growth. Figure 6a presents a representative calculation
 364 for a transient recorded in aerated pH 1.5 and arbitrarily selected among all transients available. The

365 exponential decay follows precisely the experimental decay for τ_{2D} equal to 0.13 s and τ_{3D} equal to
366 0.96 s. In this example, the nucleation current prevails until 0.22 s, whereas the thickening current
367 becomes the majority between 0.22 s and 3.5 s. Note that a similar analysis was done on other
368 transients, and the range of predominance of the 3D mechanism depends on the time constants.
369 Whatever the test, the transient fits present an R^2 higher than 0.98. Consequently, the fit process is
370 considered to characterize repassivation kinetics [5].

371



372



373

374 Figure 6a) repassivation transient (n° 2226) in aerated solution pH1.5 and fitted by Equation 1. b)
 375 determination of the growth mechanism (Equation 2) in the prevalence domain of the 3D
 376 mechanism.

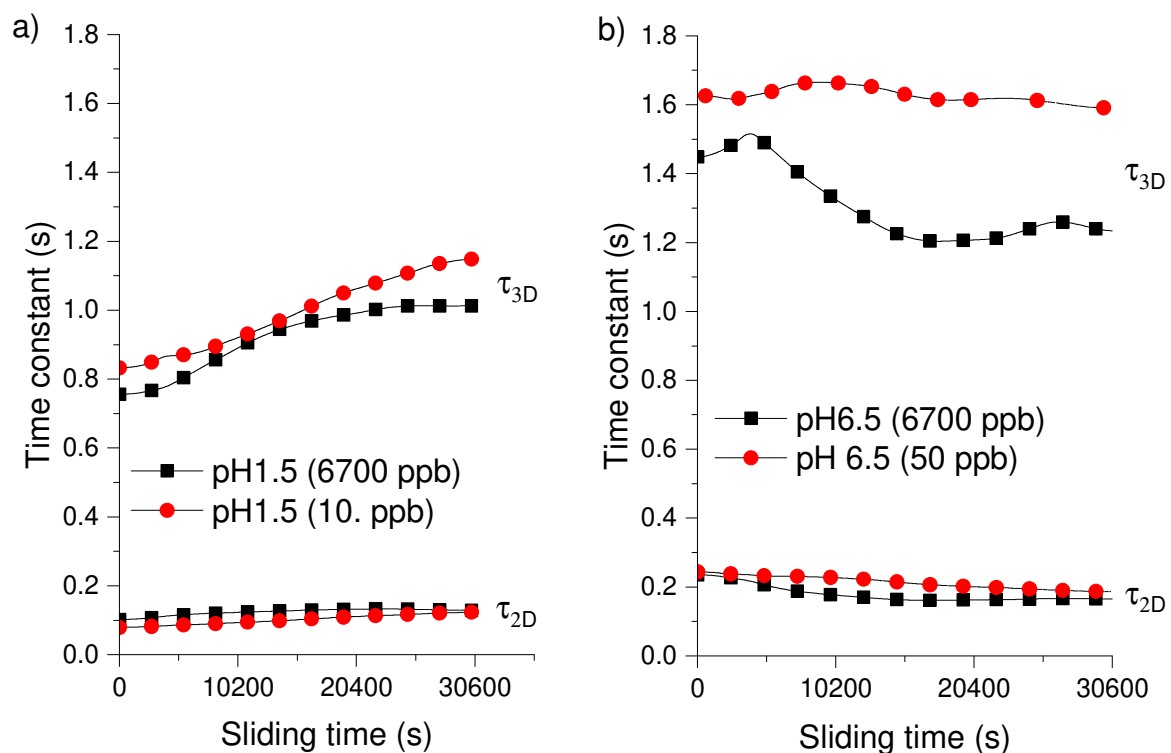
377

378 **Figure 7** reports the variations of both τ_{2D} and τ_{3D} as a function of the chemistry of the solution (pH
 379 and O_2 content). The time constants are significantly higher than those found by Déforge et al. [47] et

380 Berradja [48] for the kinetic of the recharging of the double-layer capacitance. Therefore, τ_{2D} and τ_{3D}
381 are used to describe the repassivation kinetic (Eq.1). At first, the germination time constants τ_{2D} , are
382 equal to 0.09 s and 0.23 s in acid and neutral solution, respectively. For Lavigne et al. [49], the rebuilt
383 of the film depends on the electrical charge, which linked to the overpotential. The faster
384 germination at pH 1.5 is then consistent with the higher drop of potential and the most significant
385 amplitude of current observed at this pH (Figure 3). After a certain lapse of time, the time constants
386 increase slightly until 0.13 s in acid, whereas they decrease slowly until 0.17 s in neutral solution.
387 Note that this trend is less critical than for τ_{3D} . Moreover, the elimination of O_2 has no significant
388 effect on τ_{2D} if the error scales are considered. Thus, it confirms that the film nucleation is not based
389 on the dissolved oxygen reactivity but rather on the oxygen available from the hydrolysis of water
390 [19,50,51]. Regarding τ_{3D} , the thickening rate remains faster in acidic solution. Figure 6 also shows an
391 increase of the time constants at pH 1.5, whereas τ_{3D} reduces or remains stable in neutral solution. A
392 detrimental effect of O_2 elimination is also observed with a strong impact in neutral solution.

393 These results suggest no effect of O_2 on the oxide nucleation controlled by either the Chromium or
394 Iron reactivities and the stability of the oxide products in solution. When pH increases to 6.5, iron
395 interplays with the chromium in the germination of the oxide, and this rivalry reduces the kinetic of
396 the passive film formation. The hydroxide structure favored in neutral pH may reduce the nucleation
397 rate in film mechanisms such as the one proposed by Okamoto [50]. Since the germination times
398 vary slowly with the sliding, it can be assumed that the increase of the surface deformation plays a
399 role in the oxide germination. On the one hand, the plastic deformation of the wear track may act
400 negatively on the formation of chromium oxide nuclei. On the other hand, iron and chromium
401 species (oxide and/or hydroxide) could germinate easily on the worn surface at pH 6.5 without
402 significant effect of the surface deformation. Since the affinity of oxygen for the chromium is higher
403 than the iron, the thickening rate is faster in acidic solution. Therefore, the kinetics of the oxide
404 growth act to wear, causing faster repassivation and higher loss of mater (Table 1). In the third body
405 concept, this indicates that the fragmentation of a mature passive film could generate harder debris

406 and increase the wear [10]. [10,52]. A second consequence of the **slow down** of the film formation is
 407 the increase of the chemical wear in the total wear, as **reported in Table 1**. The difference of growth
 408 rate between the aerated and the deaerated solutions could be explained either by a modification of
 409 the growth mechanism or complex interaction between the oxide film composition, the plastically
 410 deformed layer (migration/diffusion of defects), the potential drop between the bulk and the
 411 solution [53]. The experiments performed in this work are not **able to answer the second hypothesis**,
 412 **by using an** analysis of the current transients during the repassivation period can help to conclude
 413 about a modification of the growth mechanism with (i) the pH and (ii) the O₂ content in solution.
 414



415
 416 Figure 7. Variation of time constants for the oxide nucleation (τ_{2D}) and growth (τ_{3D}) in a) acid and b)
 417 neutral solutions during tribocorrosion experiments. Values calculated during the repassivation
 418 process with an average R² value of 0.98 for each fit. Error on time constant at 0.02 s and are not
 419 reported on the graph.

420

421 **3.5. Identification of growth mechanisms from repassivation current transient analysis.**

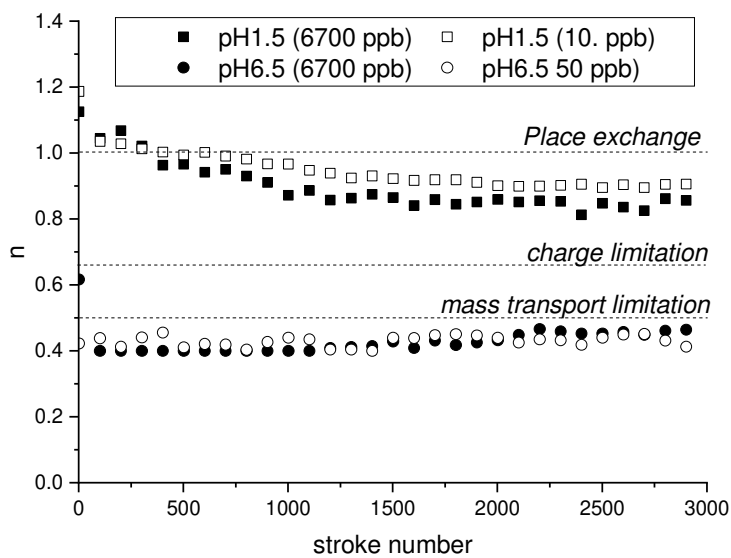
422 The determination of the growth mechanism is based on the current versus time curve fitting with
423 Equation 5 [18,54,55]. In this model, the parameter n characterizes the mechanism [54]. When the
424 film grows according to the place exchange model, n is equal to 1 [56]. On the other hand, a charge
425 or mass controlled mechanisms are defined by either 0.6 or 0.5, respectively [57,58].

$$426 \quad i = k \cdot t^{-n} \quad \text{Equation.5}$$

427 Figure 6b reports the domain of validity of the fit for the transient number 2226 recorded in aerated
428 pH 1.5 solution. It corresponds to the prevalence of the 3D current. Note that this domain is adjusted
429 for each transient as the repassivation rate evolves slightly with the sliding (Figure 7). Whatever the
430 test, determinations of n are obtained with an average R^2 value of 0.98, which indicates an excellent
431 agreement between the power-law model and the experimental decrease of the current.

432 In acidic solution, the parameter n slightly decreases from 1 to 0.85 (Figure 8), which suggests an
433 influence of the surface deformation on the growth mechanism. Until 1×10^4 s, the metal-oxygen
434 exchange in a given row (Sato model) remains the primary process. When the surface reactivity
435 becomes sensitive to the mechanical deformation of the wear track, the film growth competes with
436 the injection and annihilation of dislocations induced by the mechanical degradation [55,59].
437 Therefore, a mixed mechanism takes place with a place exchange model related to the chromium
438 reactivity in acidic solution and a charge control limitation originating to the migration/diffusion of
439 mechanical defects [57]. In a neutral solution, the parameter n remains constant at 0.45. This value
440 closed to 0.5 defines a growth mechanism under a mass transport limitation slightly affected by the
441 surface damage. Whatever the pH, a variation of the O_2 level in the cell does not affect the oxide
442 growth mechanism. Therefore, the film formation is not directly driven by the dissolved dioxygen but
443 instead induced by the oxygen available from the hydrolysis of water [19,50]. This observation is
444 consistent with the **Interface Field Model or the Point Defects Model** models for whom the
445 decomposition of the water at the film/solution interface is one or a crucial step in the passivation
446 mechanism, respectively. The mass transport limitation in the neutral solution can be related to the

447 iron injection into the oxide film formation rather than the dissolved dioxygen. These observations
 448 confirm the second hypothesis enounced previous where the oxide thickening has to be understood
 449 in terms of the oxide layer in interaction with the plastically deformed layer generated during sliding
 450 [5,59]. Further investigations are planned to discuss the role of the environment on the passive film
 451 composition and the surface structuration. Note that they should be performed in an environment
 452 where the chemical wear contribution should be higher.



453

454 Figure 8. Variation of the parameter n , related to the mechanism of the oxide growth according to
 455 the solution pH and the oxygen level. Determinations of n are obtained with an average R^2 value of
 456 0.98.

457

458 4. Conclusions

459 Tribo-electrochemical behavior of a DSS2205 duplex stainless in galvanic coupling with a graphite
 460 counter electrode was studied. The reactivity description was achieved with the analysis of the
 461 current transients in acidic and neutral solutions and the control of the dissolved dioxygen.

462 Results can be summarized as follow:

- 463 - The wear increases with the pH decreases. However, the dissolved dioxygen elimination
464 mitigates the loss of mater.
- 465 - The chemical wear represents a few percentages in the total wear. Thus, the mechanic
466 dominates the material loss. Even if abrasive wear occurs, wear track morphologies change
467 with the solution meaning that the solution chemistry also plays a role.
- 468 - The dissolution rate increases with the pH decreases. As the dissolution is a charge transfer
469 mechanism, dissolved oxygen does not affect even if the potentials under sliding are more
470 cathodic in the absence of O₂
- 471 - The oxide nucleation only depends on pH. The oxide germination is faster as the dissolution
472 is stronger in pH 1.5. The same trend is observed for the thickening step. However, the wear
473 reduces as the passive film rebuilt is slower in the absence of O₂.
- 474 - The oxide growth mechanism is only controlled by pH. In acid solution, the oxide thickening
475 should follow the place exchange model, whereas it is under a mass transport limitation in
476 neutral solution. Since O₂ concentration does not affect the mechanism, the mass transport
477 limitation is attributed to the iron injection in the oxide film at pH 6.5.

478

- 480 [1] P. Keller, H.-H. Strehblow, XPS investigations of electrochemically formed passive layers on
481 Fe/Cr-alloys in 0.5 M H₂SO₄, *Corros. Sci.* 46 (2004) 1939–1952. doi:10.1016/j.corsci.2004.01.007.
- 482 [2] P. Schmuki, From Bacon to barriers: a review on the passivity of metals and alloys, *J. Solid State*
483 *Electrochem.* 6 (2002) 145–164. doi:10.1007/s100080100219.
- 484 [3] T.A. Adler, R.P. Walters, Repassivation of 304 Stainless Steel Investigated with a Single Scratch
485 Test, *Corrosion.* 49 (1993) 399–408. doi:10.5006/1.3316067.
- 486 [4] G.T. Burstein, P.I. Marshall, Growth of passivating films on scratched 304L stainless steel in
487 alkaline solution, *Corros. Sci.* 23 (1983) 125–137. doi:10.1016/0010-938X(83)90111-7.
- 488 [5] V. Dalbert, N. Mary, B. Normand, C. Verdu, T. Douillard, S. Saedlou, The effects of
489 microstructures and repassivation kinetics on the tribocorrosion resistance of ferrite and ferrite-
490 martensite stainless steels, *Wear.* 420–421 (2019) 245–256. doi:10.1016/j.wear.2018.10.023.
- 491 [6] S. Mischler, A. Spiegel, D. Landolt, The role of passive oxide films on the degradation of steel in
492 tribocorrosion systems, *Wear.* 225–229, Part 2 (1999) 1078–1087. doi:10.1016/S0043-
493 1648(99)00056-3.
- 494 [7] C.-O.A. Olsson, D. Landolt, Passive films on stainless steels—chemistry, structure and growth,
495 *Electrochimica Acta.* 48 (2003) 1093–1104. doi:10.1016/S0013-4686(02)00841-1.
- 496 [8] P. Jemmely, S. Mischler, D. Landolt, Electrochemical modeling of passivation phenomena in
497 tribocorrosion, *Wear.* 237 (2000) 63–76. doi:10.1016/S0043-1648(99)00314-2.
- 498 [9] C. Brin, J.-P. Rivière, J.-P. Eymery, J.-P. Villain, Structural Characterization of Wear Debris
499 Produced During Friction Between Two Austenitic Stainless Steel Antagonists, *Tribol. Lett.* 11
500 (2001) 127–132. doi:10.1023/A:1016612718139.
- 501 [10] D. Landolt, S. Mischler, M. Stemp, S. Barril, Third body effects and material fluxes in
502 tribocorrosion systems involving a sliding contact, *Wear.* 256 (2004) 517–524.
503 doi:10.1016/S0043-1648(03)00561-1.
- 504 [11] P. Jemmely, S. Mischler, D. Landolt, Tribocorrosion behaviour of Fe–17Cr stainless steel in acid
505 and alkaline solutions, *Tribol. Int.* 32 (1999) 295–303. doi:10.1016/S0301-679X(99)00051-1.
- 506 [12] M. Ruiz-Andres, A. Conde, J. de Damborenea, I. Garcia, Friction and wear behaviour of dual
507 phase steels in discontinuous sliding contact conditions as a function of sliding speed and contact
508 frequency, *Tribol. Int.* 90 (2015) 32–42. doi:10.1016/j.triboint.2015.03.038.
- 509 [13] I. García, D. Drees, J.P. Celis, Corrosion-wear of passivating materials in sliding contacts based on
510 a concept of active wear track area, *Wear.* 249 (2001) 452–460. doi:10.1016/S0043-
511 1648(01)00577-4.
- 512 [14] M. Salasi, G. Stachowiak, G. Stachowiak, Tribo-electrochemical behaviour of 316L stainless steel:
513 the effects of contact configuration, tangential speed, and wear mechanism, *Corros. Sci.* (n.d.).
514 doi:10.1016/j.corsci.2015.05.009.
- 515 [15] M. Keddam, P. Ponthiaux, V. Vivier, Tribo-electrochemical impedance: A new technique for
516 mechanistic study in tribocorrosion, *Electrochimica Acta.* (2013).
517 doi:10.1016/j.electacta.2013.08.186.
- 518 [16] A. Berradja, F. Bratu, L. Benea, G. Willems, J.-P. Celis, Effect of sliding wear on tribocorrosion
519 behaviour of stainless steels in a Ringer's solution, *Wear.* 261 (2006) 987–993.
520 doi:10.1016/j.wear.2006.03.003.
- 521 [17] L. Fedrizzi, S. Rossi, F. Bellei, F. Deflorian, Wear–corrosion mechanism of hard chromium
522 coatings, *Wear.* 253 (2002) 1173–1181. doi:10.1016/S0043-1648(02)00254-5.
- 523 [18] C.-O.A. Olsson, M. Stemp, Modelling the transient current from two rubbing electrode
524 configurations: insulating pin on metal substrate and metal pin on insulating substrate,
525 *Electrochimica Acta.* 49 (2004) 2145–2154. doi:10.1016/j.electacta.2003.12.041.
- 526 [19] J.R. Goldberg, J.L. Gilbert, Electrochemical response of CoCrMo to high-speed fracture of its
527 metal oxide using an electrochemical scratch test method, *J. Biomed. Mater. Res.* 37 (1997) 421–
528 431. doi:10.1002/(SICI)1097-4636(19971205)37:3<421::AID-JBM13>3.0.CO;2-E.

- 529 [20] B.A. Okorie, Kinetics of Formation of Passive Oxide Films on Corrosion-Resistant Fe-Cr Thin Films,
530 J. Electrochem. Soc. 130 (1983) 290. doi:10.1149/1.2119696.
- 531 [21] V. Vignal, N. Mary, P. Ponthiaux, F. Wenger, Influence of friction on the local mechanical and
532 electrochemical behaviour of duplex stainless steels, Wear. 261 (2006) 947–953.
533 doi:10.1016/j.wear.2006.03.002.
- 534 [22] M. Moine, N. Mary, B. Normand, L. Peguet, A. Gaugain, H.N. Evin, Tribo electrochemical behavior
535 of ferrite and ferrite–martensite stainless steels in chloride and sulfate media, Wear. 292–293
536 (2012) 41–48. doi:10.1016/j.wear.2012.06.001.
- 537 [23] M. Stemp, S. Mischler, D. Landolt, The effect of contact configuration on the tribocorrosion of
538 stainless steel in reciprocating sliding under potentiostatic control, Corros. Sci. 45 (2003) 625–
539 640. doi:10.1016/S0010-938X(02)00136-1.
- 540 [24] A. de Frutos, M.A. Arenas, G.G. Fuentes, R.J. Rodríguez, R. Martínez, J.C. Avelar-Batista, J.J. de
541 Damborenea, Tribocorrosion behaviour of duplex surface treated AISI 304 stainless steel, Surf.
542 Coat. Technol. 204 (2010) 1623–1630. doi:10.1016/j.surfcoat.2009.10.039.
- 543 [25] V. Dalbert, N. Mary, B. Normand, C. Verdu, T. Douillard, S. Saedlou, The effects of
544 microstructures and repassivation kinetics on the tribocorrosion resistance of ferrite and ferrite-
545 martensite stainless steels, Wear. (2018). doi:10.1016/j.wear.2018.10.023.
- 546 [26] Z. Doni, A.C. Alves, F. Toptan, J.R. Gomes, A. Ramalho, M. Buciumeanu, L. Palaghian, F.S. Silva,
547 Dry sliding and tribocorrosion behaviour of hot pressed CoCrMo biomedical alloy as compared
548 with the cast CoCrMo and Ti6Al4V alloys, Mater. Des. 1980-2015. 52 (2013) 47–57.
549 doi:10.1016/j.matdes.2013.05.032.
- 550 [27] J. Qu, J.J. Truhan, An efficient method for accurately determining wear volumes of sliders with
551 non-flat wear scars and compound curvatures, Wear. 261 (2006) 848–855.
552 doi:10.1016/j.wear.2006.01.009.
- 553 [28] P.-Q. Wu, J.-P. Celis, Electrochemical noise measurements on stainless steel during corrosion–
554 wear in sliding contacts, Wear. 256 (2004) 480–490. doi:10.1016/S0043-1648(03)00558-1.
- 555 [29] J.F. Chen, W.F. Bogaerts, Electrochemical Emission Spectroscopy for Monitoring Uniform and
556 Localized Corrosion, CORROSION. 52 (1996) 753–759. doi:10.5006/1.3292068.
- 557 [30] N. Papageorgiou, S. Mischler, Electrochemical Simulation of the Current and Potential Response
558 in Sliding Tribocorrosion, Tribol. Lett. 48 (2012) 271–283. doi:10.1007/s11249-012-0022-9.
- 559 [31] A.C. Vieira, L.A. Rocha, N. Papageorgiou, S. Mischler, Mechanical and electrochemical
560 deterioration mechanisms in the tribocorrosion of Al alloys in NaCl and in NaNO₃ solutions,
561 Corros. Sci. 54 (2012) 26–35. doi:10.1016/j.corsci.2011.08.041.
- 562 [32] D. Landolt, S. Mischler, M. Stemp, Electrochemical methods in tribocorrosion: a critical appraisal,
563 Electrochimica Acta. 46 (2001) 3913–3929. doi:10.1016/S0013-4686(01)00679-X.
- 564 [33] J.P. Popić, D.M. Dražić, Electrochemistry of active chromium: Part II. Three hydrogen evolution
565 reactions on chromium in sulfuric acid, Electrochimica Acta. 49 (2004) 4877–4891.
566 doi:10.1016/j.electacta.2004.05.042.
- 567 [34] Z. Feng, X. Cheng, C. Dong, L. Xu, X. Li, Effects of dissolved oxygen on electrochemical and
568 semiconductor properties of 316L stainless steel, J. Nucl. Mater. 407 (2010) 171–177.
569 doi:10.1016/j.jnucmat.2010.10.010.
- 570 [35] P. Schmutz, D. Landolt, In-situ microgravimetric studies of passive alloys: potential sweep and
571 potential step experiments with Fe–25Cr and Fe–17Cr–33Mo in acid and alkaline solution,
572 Corros. Sci. 41 (1999) 2143–2163. doi:10.1016/S0010-938X(99)00038-4.
- 573 [36] S. Haupt, H.-H. Strehblow, A combined surface analytical and electrochemical study of the
574 formation of passive layers on FeCr alloys in 0.5 M H₂SO₄, Corros. Sci. 37 (1995) 43–54.
575 doi:10.1016/0010-938X(94)00104-E.
- 576 [37] S. Tanaka, N. Hara, K. Sugimoto, Corrosion characteristics of Fe₂O₃·Cr₂O₃ artificial passivation
577 films under potentiostatic control, Mater. Sci. Eng. A. 198 (1995) 63–69. doi:10.1016/0921-
578 5093(95)80059-4.

- 579 [38] C.-O.A. Olsson, D. Landolt, Film Growth during Anodic Polarization in the Passive Region on 304
580 Stainless Steels with Cr, Mo, or W Additions Studied with EQCM and XPS, *J. Electrochem. Soc.*
581 148 (2001) B438. doi:10.1149/1.1404969.
- 582 [39] H.H. Uhlig, Critical pH and Critical Current Density for Passivity in Metals, *J. Electrochem. Soc.* 108
583 (1961) 327. doi:10.1149/1.2428081.
- 584 [40] N. Espallargas, R. Johnsen, C. Torres, A.I. Muñoz, A new experimental technique for quantifying
585 the galvanic coupling effects on stainless steel during tribocorrosion under equilibrium
586 conditions, *Wear.* 307 (2013) 190–197. doi:10.1016/j.wear.2013.08.026.
- 587 [41] S. Cao, S. Mischler, Modeling tribocorrosion of passive metals – A review, *Curr. Opin. Solid State*
588 *Mater. Sci.* (2018). doi:10.1016/j.cossms.2018.06.001.
- 589 [42] A.C. Vieira, A.R. Ribeiro, L.A. Rocha, J.P. Celis, Influence of pH and corrosion inhibitors on the
590 tribocorrosion of titanium in artificial saliva, *Wear.* 261 (2006) 994–1001.
591 doi:10.1016/j.wear.2006.03.031.
- 592 [43] W. Kuang, X. Wu, E.-H. Han, Influence of dissolved oxygen concentration on the oxide film
593 formed on 304 stainless steel in high temperature water, *Corros. Sci.* 63 (2012) 259–266.
594 doi:10.1016/j.corsci.2012.06.007.
- 595 [44] Y.H. Huang, T.C. Zhang, Effects of dissolved oxygen on formation of corrosion products and
596 concomitant oxygen and nitrate reduction in zero-valent iron systems with or without aqueous
597 Fe²⁺, *Water Res.* 39 (2005) 1751–1760. doi:10.1016/j.watres.2005.03.002.
- 598 [45] K. Asami, K. Hashimoto, S. Shimodaira, XPS determination of compositions of alloy surfaces and
599 surface oxides on mechanically polished iron-chromium alloys, *Corros. Sci.* 17 (1977) 713–723.
600 doi:10.1016/0010-938X(77)90067-1.
- 601 [46] J. Camra, E. Bielańska, A. Bernasik, K. Kowalski, M. Zimowska, A. Białas, M. Najbar, Role of Al
602 segregation and high affinity to oxygen in formation of adhesive alumina layers on FeCr alloy
603 support, *Catal. Today.* 105 (2005) 629–633. doi:10.1016/j.cattod.2005.06.015.
- 604 [47] D. Déforge, F. Huet, R.P. Nogueira, P. Ponthiaux, F. Wenger, Electrochemical Noise Analysis of
605 Tribocorrosion Processes under Steady-State Friction Regime, 62 (2006) 514–521.
606 doi:10.5006/1.3279910.
- 607 [48] A. Berradja, D. Déforge, R.P. Nogueira, P. Ponthiaux, F. Wenger, J.-P. Celis, An electrochemical
608 noise study of tribocorrosion processes of AISI 304 L in Cl⁻ and media, 39 (2006) 3184–3192.
609 doi:10.1088/0022-3727/39/15/S08.
- 610 [49] O. Lavigne, C. Alemany-Dumont, B. Normand, S. Berthon-Fabry, R. Metkemeijer, Thin chromium
611 nitride PVD coatings on stainless steel for conductive component as bipolar plates of PEM fuel
612 cells: Ex-situ and in-situ performances evaluation, *Int. J. Hydrog. Energy.* 37 (2012) 10789–10797.
613 doi:10.1016/j.ijhydene.2012.04.035.
- 614 [50] G. Okamoto, Passive film of 18-8 stainless steel structure and its function, *Corros. Sci.* 13 (1973)
615 471–489. doi:10.1016/0010-938X(73)90031-0.
- 616 [51] H. Abd-El-Kader, S.M. El-Raghy, Wear-corrosion mechanism of stainless steel in chloride media,
617 *Corros. Sci.* 26 (1986) 647–653. doi:10.1016/0010-938X(86)90029-6.
- 618 [52] S. Mischler, Electrochemical control of wear: a third body approach, in: M.P. D. Dowson (Ed.),
619 *Tribol. Ser.*, Elsevier, 2003: pp. 47–56.
620 <http://www.sciencedirect.com/science/article/pii/S0167892203801189> (accessed October 9,
621 2013).
- 622 [53] D.D. Macdonald, The history of the Point Defect Model for the passive state: A brief review of
623 film growth aspects, *Electrochimica Acta.* 56 (2011) 1761–1772.
624 doi:10.1016/j.electacta.2010.11.005.
- 625 [54] D.D. MacDonald, B. Roberts, A potentiostatic transient study of the passivation of carbon steel in
626 1 M NaOH, *Electrochimica Acta.* 23 (1978) 557–564. doi:10.1016/0013-4686(78)85036-1.
- 627 [55] R.W. Staehle, Transient stability of passive films in aqueous solutions, *Corros. Sci.* 49 (2007) 7–
628 19. doi:10.1016/j.corsci.2006.05.006.
- 629 [56] S. Asakura, K. Nobe, Kinetics of Anodic Processes on Iron in Alkaline Solutions, *J. Electrochem.*
630 *Soc.* 118 (1971) 536–541. doi:10.1149/1.2408106.

- 631 [57] D.A. Vermilyea, On the Theory of Electrolytic Crystal Growth, *J. Chem. Phys.* 25 (1956) 1254–
632 1263. doi:10.1063/1.1743189.
- 633 [58] J.W. Tester, H.S. Isaacs, Diffusional Effects in Simulated Localized Corrosion, *J. Electrochem. Soc.*
634 122 (1975) 1438–1445. doi:10.1149/1.2134039.
- 635 [59] J. Perret, E. Boehm-Courjault, M. Cantoni, S. Mischler, A. Beaudouin, W. Chitty, J.-P. Vernot,
636 EBSD, SEM and FIB characterisation of subsurface deformation during tribocorrosion of stainless
637 steel in sulphuric acid, *Wear.* 269 (2010) 383–393. doi:10.1016/j.wear.2010.04.023.
- 638